Volume xx (200y), Number z, pp. 1–13

Parametric Skeletons with Reduced Soft-Tissue Deformations

Javier Tapia, Cristian Romero, Jesús Pérez, Miguel A. Otaduy

Universidad Rey Juan Carlos, Madrid, Spain

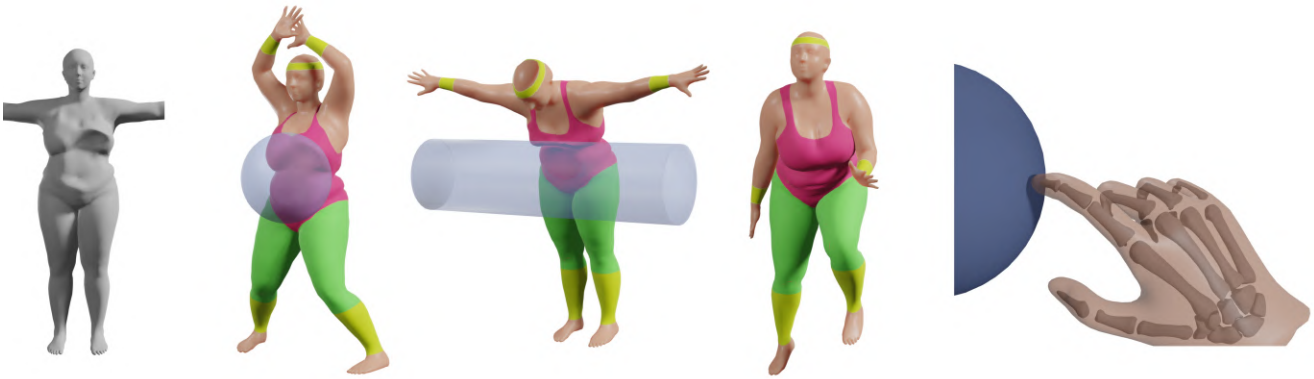

Figure 1: *We augment parametric skeletal models with reduced soft-tissue deformations. We formulate dynamics in an unposed reference space (left) and design a sparse biharmonic subspace to represent soft-tissue deformation. The local basis efficiently captures inertial effects and external interactions (middle) while preserving accurate data-driven static deformations depending on the skeletal pose. We demonstrate our method with realistic real-time simulations of human characters and hands (right).*

Abstract

We present a method to augment parametric skeletal models with subspace soft-tissue deformations. We combine the benefits of data-driven skeletal models, i.e., accurate replication of contact-free static deformations, with the benefits of pure physics-based models, i.e., skin and skeletal reaction to contact and inertial motion with two-way coupling. We succeed to do so in a highly efficient manner, thanks to a careful choice of reduced model for the subspace deformation. With our method, it is easy to design expressive reduced models with efficient yet accurate force computations, without the need for training deformation examples. We demonstrate the application of our method to parametric models of human bodies, SMPL, and hands, MANO, with interactive simulations of contact with nonlinear soft-tissue deformation and skeletal response.

CCS Concepts

• ***Computing methodologies*** → ***Physical simulation;***

1. Introduction

Data-driven and physics-based methods offer competing features for the animation of skeletal figures such as human bodies or hands. Data-driven methods are very fast and reproduce with high accuracy contact-free static poses. However, they do not exhibit soft-tissue deformations and skeletal reaction due to contact or inertial effects. Physics-based methods, on the other hand, are reactive and exhibit detailed soft-tissue deformations with potentially two-way coupled skeletal motion. They also produce plausible results beyond previously observed situations. However, their computational cost is considerably higher, and they have trouble accurately matching observations, due to the complexity of parameter estimation.

Our work is connected to two types of methods that try to bridge the gap between data-driven and physics-based skeletal animation. One type is hybrid simulation methods, and the other type is subspace deformation methods. Hybrid simulation methods build a

physics-based model on top of a data-driven skeletal model. As an example, some authors have extended the SMPL parametric avatar model [LMR*15] with a soft-tissue layer [KPMP*17, ROCP20]. But these hybrid methods are very costly, because resolving the geometric details of skeletal models requires high-resolution meshes.

Subspace simulation methods provide a fast way to approximate soft-tissue deformations. They build a reduced kinematic basis, while evaluating the deformation of the complete high-resolution mesh. Subspace methods have been applied to skeletal models, to augment soft-tissue dynamics in an efficient way [GOM*09, TMDK15, XB16]. Most subspace methods rely on example deformations to train two components: the reduced basis, and cubature integration samples [AKJ08]. In our experience, the generation of training data is a major complication for the effectiveness of subspace methods, and their accuracy degrades for unobserved deformations, which is easily the case in contact-rich scenarios.

In this work, we leverage recent developments on data-driven skeletal models [LMR*15, RTB17] and skinning-based subspace methods [WJBK15]. The latter provide intuitive ways to define expressive subspaces, simply by selecting handles on the target object, without the need for deformation examples. In Section 3, we present a model of reduced kinematics that combines a data-driven skeletal model and a skinning-based subspace method. For the successful conservation of accurate data-driven deformations, we build the subspace basis and formulate dynamics in the unposed reference shape. The resulting model produces effective skeletal dynamics and data-driven pose-space global static deformation, enriched with local subspace soft-tissue deformations.

In Section 4, we describe the definition of the various force models (elastic, contact, inertial) on the proposed kinematics model. Furthermore, we introduce a cubature method that exploits the interpolation scheme of skinning-based subspaces and requires no training examples. The need for training data is replaced with simple manual selection of cubature points.

We have applied our deformation method to augment the SMPL body model [LMR*15] and the MANO hand model [RTB17] with interactive, nonlinear soft-tissue deformations. We set up demonstration examples controlled by either scripted character animations or interactive hand tracking, with two-way coupling of skeletal response and soft-tissue deformation under contact scenarios, as shown in Figure 1.

2. Related Work

Since the pioneering work of Terzopoulos and Witkin [TW88], the computer graphics community has been increasingly interested in physics-based animation. Many existing articles and courses discuss the evolution and current development of deformable object simulation, e.g., [NMK*06, SB12, BS19]. We are particularly interested in subspace methods, and the different ways in which they can be combined with skeletal models.

2.1. Soft Skeletal Models

Skeletal Subspace Deformation (SSD) [MTLT89] has been extensively used for the animation of skeletal characters and objects. It consists of the transformation of the vertices of a surface mesh by non-linearly mapping a low-dimensional space of rig parameters. These so-called rigging techniques are ubiquitous in software animation packages which often include linear blend skinning and various other nonlinear deformers. The simulation of soft articulated bodies has motivated many works that enrich rigging techniques with dynamics, e.g., [CGC*02, CBC*05]. Most of these simulation methods represent the skeletal structure with an articulated body, and model the soft tissue as a continuum layer coupled to the skeleton. While the skeleton is generally kinematically animated, some works propose two-way coupling between the soft-tissue and the articulated body [LYWG13] for animation control. Even though significant efforts have been devoted to improving their efficiency [GOT*07, MZS*11, LLK19], full-space methods generally do not run at real-time rates for complex geometry. In addition, it might be challenging to produce nonlinear deformations caused by fast and large skeletal animations. Rig-space physics [HMT*12, HTC*13] address this problem by letting standard rigging take care of large skeletal deformations and formulating dynamics directly in the rig space. This approach is similar in spirit to the more general category of pose-space methods [LCF00], which define a reference shape of the skin, apply a pose-space deformation (PSD) to it, and then transform the deformed skin through rigging. While Lewis et al. [LCF00] computed the PSD through scattered-data interpolation of deformation samples, many other solutions are possible. We are particularly interested in the data-driven models SMPL [LMR*15] and MANO [RTB17], which define the PSD using blend shapes governed by the skeletal pose as well as shape parameters. Such blend shapes are fitted to accurately depict the deformation of parametric bodies and hands respectively under static poses. Kim et al. [KPMP*17] combined the SMPL model with a soft-tissue layer simulated in full space. Very recently, Romero et al. [ROCP20] further improved this method by formulating deformations in the unposed reference space to allow external interactions while preserving the accurate static data-driven deformation. In this paper, we combine the previous idea with a local deformation subspace and a custom cubature scheme to allow for real-time simulation of complex skeletal soft models.

2.2. Subspace Simulation

Subspace methods replace the degrees of freedom (DoFs) of a chosen discretization with a much smaller set of DoFs expressed in a subspace of basis vectors. This naturally accelerates simulations at the cost of losing deformation detail that cannot be captured by the subspace basis. Designing an appropriate basis has been a research interest since the early works based on linear modal analysis [KLM01, OHS03]. Later developments allowed the incorporation of non-linear phenomena [BJ05], the acceleration of force computations [AKJ08], or the adaptive combination of subspace and full-space formulations [TMDK15], among others. Recent developments in the field of subspace simulation explore the use of variational autoencoders for finding a latent-space that serves as a deformation subspace [FMD*19].

Subspace bases usually have global support, e.g., [KLM01, BJ05], meaning every DoF in the full space depends kinematically on every subspace basis vector. This is not necessarily real-

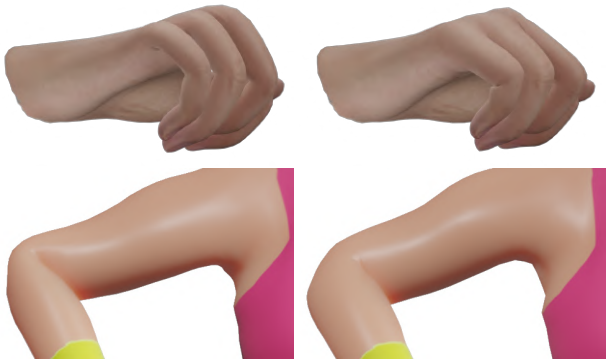

Figure 2: *This figure highlights the deformations produced by the data-driven skeletal model in our formulation (left: without pose-based blend shapes; right: with pose-based blend-shapes). Our deformation model matches exactly the data-driven result on static, contact-free poses.*

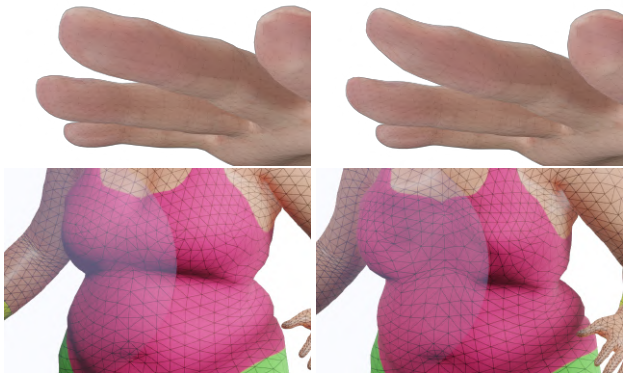

Figure 3: *On a skeletal model such as the one described in Section 3.1, contact forces are fully absorbed by the skeleton (left). With our augmented soft model described in Section 3.3, contact induces soft-tissue deformations (right).*

istic and may cause that novel interactions, which were not originally considered in the design of the subspace, produce unrealistic global artifacts. Some works have alleviated this burden using domain decomposition techniques [KJP02, BZ11, KJ11], while others directly address the design of local subspace bases. Local methods are generally based on skinning transformation handles, spatially distributed in regions of deformation interest. Some examples include the use of interpolated frames [GBFP11, FGBP11], Boussinesq static deformation response [HZ13], automatic sparse matrix computation [NVW*13], and the more recent work of Brandt et al. [BEH18], which interpolates affine transformations skinned using geodesic radial basis functions. We opt for the biharmonic generalized barycentric coordinates (BGBC) scheme of Wang et al. [WJBK15], which considers both handle points and affine frames. This method simplifies the construction of the basis, for which the user can simply select handle points on the surface of the mesh where local deformations are expected. Furthermore, explicit consideration of affine frames that are interpolated in a smooth, shape-aware manner, allows us to seamlessly combine the subspace method with a data-driven skeletal model.

Local subspace methods naturally produce sparse bases that allow for highly efficient computation of dynamic equations. When the basis vectors are smooth, this cost can be further alleviated using cubature [AKJ08, vTSSH13]. Cubature methods approximate integrals across the mesh using a small set of representative elements. This usually involves a very expensive precomputation where the optimal set is selected to match forces for some training examples. Instead we opt for a less tedious solution, in a similar spirit to [HZ13]; we propose a data-oblivious cubature scheme where energy is integrated through biharmonic interpolation.

2.3. Pose-Space Model Reduction

Model reduction has been employed before in combination with PSD. The early work by [KJP02] augmented an SSD with locally supported eigendisplacement basis functions to achieve quasi-static deformations. Many posterior works further improved this approach for the dynamic simulation of characters [GOM*09, TMDK15] or cloth [HTC*14]. Similar to our approach, these methods build their basis in an unposed configuration of the object. This might result in inaccurate deformations when skeletal configurations are far from the neutral position. Some methods like [GOM*09] and the more recent [XB16] address this problem by considering several poses for the construction of the basis. While the former constructs a single basis with per-pose PSD corrections, the latter constructs several bases at different poses and interpolates them at simulation time. We differ from these methods in that we do not intend to match the behavior of a full model for some given target poses. Instead, we aim to compute high-quality real-time deformations independently of the skeletal pose. We preserve the accurate static deformations provided by our data-driven SSD and augment them with dynamics formulated in unposed space. Contrary to data-driven model reduction, our local subspace basis is easily designed by placing point handles where deformation is needed and results in fast sparse subspace projections.

3. Augmented Skeletal Kinematics

In this section, we describe the DoFs of our skeletal soft model. The model combines features from parametric skeletal models and skinning-based reduced deformable models. We first describe these two models under a common notation, and then conclude the section discussing how we merge them.

3.1. Parametric Skeletal Model

We consider skeletal models that describe skin deformations by augmenting SSD [MTLT89] with PSD [LCF00]. These models define a reference shape of skin, apply a displacement to this reference shape as a function of the skeletal pose, and then transform the deformed skin through a combination of rigid transformations. We build on the SMPL [LMR*15] and MANO [RTB17] models, which define PSD using data-driven blend shapes governed by the skeletal pose. Moreover, SMPL and MANO also add shape-dependent blend shapes to create multi-person skeletal models of

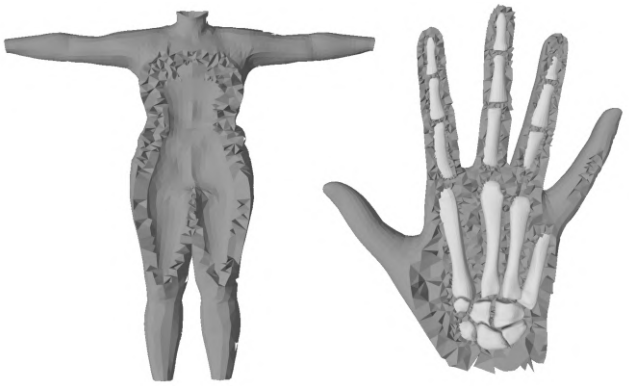

Figure 4: *Volumetric discretization of the soft-tissue layer for both the SMPL (left) and MANO (right) models. Meshes have been generated using a Delaunay tetrahedralization conformal to boundary surfaces [Si15]. In the former case, we construct the inner surface displacing the outer surface with smoothly varying thickness throughout the body. In the latter case, we use the mesh of a real hand skeleton as the inner surface. Our method only needs these meshes during preprocessing, for the computation of the subspace basis and the cubature weights.*

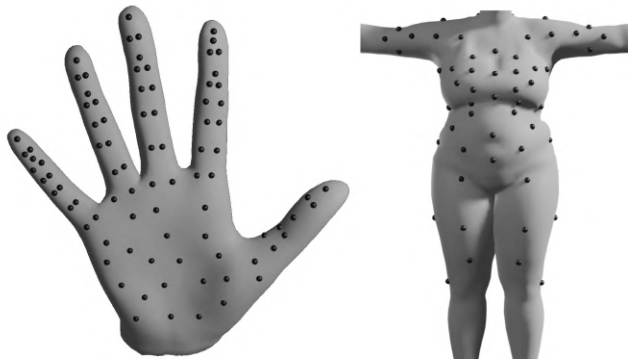

Figure 5: *This figure shows the distribution of subspace handle points defined for the body (right) and the hand (left) respectively.*

bodies and hands. Below, we show the computation of skin deformations $S_P \in \mathbb{R}^{3n}$, with n the number of surface vertices, from pose parameters $\theta \in \mathbb{R}^p$ and shape parameters $\beta \in \mathbb{R}^s$. We follow a similar notation to the original SMPL and MANO models.

$$S_P(\beta,\theta) = W(T_P(\beta,\theta), J(\beta), \theta, \mathcal{W}), \quad (1)$$
$$\text{with } T_P(\beta,\theta) = \overline{T} + B_S(\beta) + B_P(\theta).$$

$\overline{T} \in \mathbb{R}^{3n}$ represents the reference shape of the skeletal model, and $T_P \in \mathbb{R}^{3n}$ its unposed deformation. $B_S \in \mathbb{R}^{3n}$ and $B_P \in \mathbb{R}^{3n}$ represent, respectively, shape-dependent and pose-dependent blend shapes. All $\overline{T}$, T_P, S_P, B_S, and B_P represent vectors of all-vertices positions or displacements in a mesh. $W(\cdot)$ is the skeletal deformation function (linear blend skinning for SMPL and MANO), which takes as additional input the skinning weights $\mathcal{W}$. SMPL and MANO also vary the joint locations J as a function of shape parameters. In SMPL and MANO, the pose parameters θ and shape parameters β correspond, respectively, to joint angles of the skeleton and to scale factors of principal components of the reference shape.

While SMPL and MANO were originally defined as surface-only deformations, Kim et al. [KPMP*17], and later Romero et al. [ROCP20], developed volumetric extensions that fit the same formulation (1). Since we formulate dynamics in the unposed reference space (Section 4.1), we only need to evaluate the skinning transformation $W(\cdot)$ at the surface, for visualization and contact handling. However, the volumetric extensions can be adopted with no change.

The skeletal model (1) can be used as kinematic representation in dynamic simulation, endowed with joint and contact forces. The major advantage of the method is that, thanks to its data-driven nature, it reproduces contact-free deformations accurately, as shown in Figure 2. However, contact forces are fully absorbed by the skeleton, with no contact-induced soft-tissue deformation, as shown in Figure 3.

3.2. Skinning-Based Reduced Model

Several reduced models build compact and sparse bases by *skinning* the deformations of a few handle points or frames. They differ in the choice of DoFs and the construction of the basis. Some possibilities are to use rigid frames skinned with harmonic weights [GBFP11], or affine transformations skinned using geodesic radial basis functions [BEH18]. We opt for the bi-harmonic generalized barycentric coordinates (BGBC) of Wang et al. [WJBK15], which interpolate both handle points and affine frames in a smooth, shape-aware manner. The BGBC are obtained by solving a quadratic minimization on a volumetric mesh subject to interpolation constraints at handles. Wang et al. propose an objective energy based on mass-weighting a linearly precise Laplacian, and we refer to their paper for details. We discard BGBC values below a small threshold (in practice, we smoothly decay values between 0.1 and 0.03), and thus enforce local support of the basis.

Given a skeletal model, the BGBC reduced model allows us to naturally choose as handles the bones of the skeleton plus a sparse set of surface points. The model is well suited for fitting the shape (i.e., skin) of the skeletal model, as well as anatomical constraints (i.e., the bones and joints), while providing a compact deformation basis. To compute the BGBC basis, we mesh the soft-tissue volume between the outer skin surface and the inner skeleton, as shown in Figure 4. Note that we only use the volumetric meshes during preprocessing, to compute the BGBC weights as well as cubature weights (Section 4.2); we never use the volumetric meshes at runtime or to compute actual deformations.

Below, we show the computation of skin deformations $S_B \in \mathbb{R}^{3n}$ by linear combination of the positions $\phi \in \mathbb{R}^{3h}$ of h handle points and the vectorized affine transformations $A(\theta) \in \mathbb{R}^{12b}$ of b handle bones with pose θ.

$$S_B(\phi,\theta) = U_\phi \phi + U_\theta A(\theta). \quad (2)$$

$U_\phi \in \mathbb{R}^{3n\times 3h}$ and $U_\theta \in \mathbb{R}^{3n\times 12b}$ represent, respectively, the basis

vectors of handle points and handle bones, and store the BGBC of all handles.

The reduced model (2) can be used as kinematic representation in dynamic simulation, endowed with an FEM elasticity model, as well as joint and contact forces. Figure 5 shows the distribution of handle points manually selected all over the surface of the hand and the body for the examples shown in the paper. The major advantage of the method is that contact produces both skeletal reaction and soft-tissue deformation, with natural two-way coupling. However, deformations are governed solely by physics, making it very hard to match real deformation examples.

3.3. Combined Model

Next, we present our skeletal model augmented with reduced soft-tissue deformations, by combining the two models presented before. We represent the effect of bone transformations using the parametric skeletal model, i.e., through the pose blend-shapes $B_p(\theta)$ and the skinning transformation $W(\cdot)$. This provides a pose-dependent soft-tissue deformation that realistically depicts data-driven static deformation and with skeletal dynamics due to contact. In addition, we aim to achieve flesh deformations due to contact or inertia, while still preserving the accurate data-driven static deformation of the parametric skeletal model. Thus, we formulate reduced soft-tissue deformations S_B in the unposed reference shape, to capture deviations from the parametric skeletal model instead of full deformations. Our model enables simple construction of anthropomorphic models that match both flesh and bone geometry, while supporting large joint rotations. This is a complex goal for typical models that evaluate world-space deformations, because the narrow space between bones is heavily deformed under joint rotations. With our unposed deformation model, joint rotations do not cause any difficulty.

Our design choices result in ignoring the bone transformations in the reduced deformation model, i.e., $A(\theta) = 0$ in (2), since the bones remain fixed in the reference shape, but their effect is captured by the parametric skeletal model. As a result, our augmented skeletal model defines soft-tissue deformations $S \in \mathbb{R}^{3n}$ as

$$S(\phi,\theta) = W(T(\phi,\theta), J(\beta_0), \theta, \mathcal{W}), \quad \text{with } T(\phi,\theta) = \overline{T} + B_S(\beta_0) + B_P(\theta) + U_\phi \phi. \tag{3}$$

The DoFs of the model are the handle points ϕ and the skeletal pose θ. The reduced deformation $U_\phi \phi$ is evaluated on a volumetric mesh on the unposed reference shape. However, as already discussed in Section 3.1, in our implementation the rest of the model, and hence S, is evaluated only on the surface. We fix the shape parameters $\beta = \beta_0$ to create the model for a given (but arbitrary) skeletal shape. Then, the joint locations and the shape-based blend shapes remain fixed during the simulation. Note also that, even though the bone basis vectors U_θ can be ignored in the runtime simulation, the BGBC basis must be computed with both point and bone basis vectors U_ϕ and U_θ. This ensures that bones do not suffer soft-tissue deformation.

In the next section, we discuss how we endow the combined kinematics representation (3) with elastic and inertial models for dynamic simulation. As shown in Figure 6, our model enjoys the advantages of both the parametric skeletal model and the reduced deformation model; it matches static contact-free deformations accurately, and contact produces both skeletal reaction and soft-tissue deformation, with natural two-way coupling.

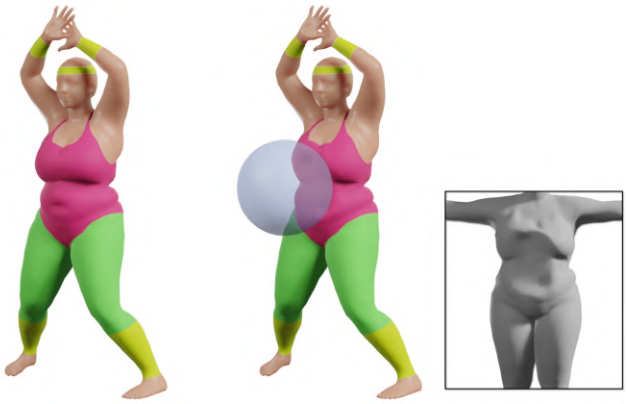

Figure 6: *Our soft skeleton body model matches static data-driven deformations accurately for a given pose (left). When in contact with an external object it produces a dynamic response with two-way coupling (right). Soft-tissue deformation is clearly noticeable in the unposed reference shape (inset). Local static deformations due to the pose blend shape (e.g., arm bulging) apply independently of external interactions.*

4. Soft Skeleton Dynamics

The augmented skeletal model described in the previous section is capable of generating skeletal animations with soft-tissue deformations. However, to generate these deformations in a physics-based simulation, we need to define force models, as well as dynamic equations that relate those forces to the motion of the skeletal and soft-tissue DoFs. We start with our formulation of reduced deformation mechanics in unposed space, followed by a novel cubature scheme that enables efficient evaluation of energies, forces and Jacobians. We complement the deformation model with a description of skeletal forces, contact handling, and the formulation and solution of dynamics.

4.1. Unposed Deformation

We measure soft-tissue deformations as deviations from the parametric skeletal motion. To this end, we require two ingredients. One is to define displacements in unposed space $U_\phi \phi$ as in (3). The other one is to define elastic energy solely based on these displacements.

Let us define a point on the reference shape as $X \in \overline{T}$. For this point, we define the rest position after adding the shape and pose blend shapes, $\bar{x}(X) = X + B_S(\beta_0, X) + B_P(\theta, X)$. And we also define the soft-tissue deformation as the unposed displacement from this rest position, $u(X) = U_\phi(X)\phi$, which yields the unposed deformation $T(X) = \bar{x}(X) + u(X)$.

Based on these definitions, we compute an unposed deformation gradient $F = \nabla_{\bar{x}} T = \nabla_X (\bar{x} + u) = I + \nabla_X U_\phi \phi$. This definition of

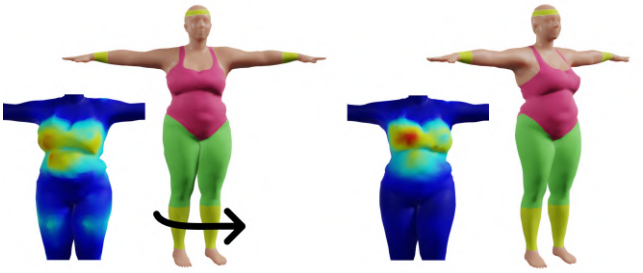

Figure 7: *Our handling of inertial forces correctly captures soft-tissue deformations induced by the skeletal motion. The picture shows two frames of an animation with a character subject to rotational acceleration (left) and deceleration (right) in the vertical axis, and the resulting colormap of soft-tissue deformations.*

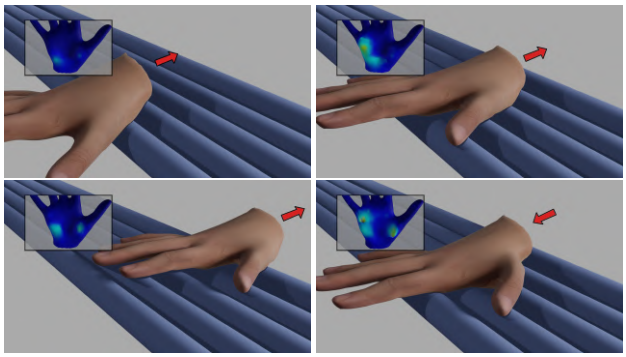

Figure 8: *A parametric approximation of the hand is realistically deformed due to skeletal poses and contact with objects. The picture shows four frames of an animation sequence and a colormap with the corresponding vertex displacements in unposed space (insets). Sliding over a structure of fine cylinders produces ripples on the palm (see supplementary video).*

the deformation gradient resembles the one recently proposed by Romero et al. [ROCP20]. However, they discretized kinematics using world positions, not unposed displacements, hence they had to explicitly compute the inverse skinning transformation of positions to compute the deformation gradient. The use of the deformation gradient allows the adoption of a large family of hyperelastic material models, and the derivation of elastic forces from the stress metric [SB12]. Given a generic elastic energy density of the form $\Psi(F)$, elastic forces on the handle points are computed as

$$\nabla_\phi \Psi = \nabla_F \Psi \cdot \nabla_X U_\phi, \tag{4}$$

where $\nabla_F \Psi$ is the First Piola-Kirchhoff stress, and $\nabla_X U_\phi$ denotes the gradient of basis vectors w.r.t. the reference shape. In our dynamics solver, we also require force Jacobians, which in turn use the Hessian of the elastic energy.

As evident from the expression above, our deformation model does not affect the skeletal pose θ. In other words, a static change of skeletal pose does not produce additional soft-tissue deformation, and the skin surface is controlled solely by the parametric model, as desired. However, as shown in Figure 7 and Figure 8, the presence of dynamic inertial terms and external contacts does produce an effect on the deformation of the soft-tissue.

In our examples, we have used a nonlinear material model that includes anisotropy and saturation [ROCP20]. Nonlinearities enable rich yet robust deformation of skin, in particular when the soft-tissue layer occupies a narrow space between the skin surface and the bones [PCH*13]. In practice, we have clamped the saturation term in the material model, to limit its highly nonlinear effect. We found that very high saturation values could require more than one Newton iteration in the backward Euler solve (see Section 4.5), and this had a significant impact on performance.

4.2. Data-Oblivious BGBC Cubature

The deformation model described above must be integrated on the whole soft tissue to compute elastic forces on the handle points. To this end, we consider the volumetric tetrahedral meshes shown in Figure 4 and use the finite element method (FEM) to discretize the continuous formulation in (4). With reduced models, the runtime cost is dominated by the computation and assembly of energy gradients and Hessians on all mesh elements and/or quadrature points, each of which must be projected onto the reduced space through the basis matrix as in (4). When the basis vectors are smooth, this cost can be alleviated thanks to cubature methods [AKJ08, vTSSH13]. They rely on the approximation of the energy, its gradient and Hessian as weighted sums of evaluations at a sparse set of points.

Typical cubature methods use deformation examples to optimize cubature point locations and cubature weights. However, the generation of representative training examples is a challenging task. Instead, we propose a data-oblivious cubature method based on the construction of an interpolation scheme on the skeletal model. We sample cubature points uniformly, construct an interpolation scheme for the elastic energy and its derivatives, and then derive cubature weights automatically by integrating the basis functions of the interpolation scheme.

Let us assume a set of cubature points $\{X_i\}$, sampled on the reference shape of the soft-tissue portion of the skeletal model, i.e., excluding the bones. We will discuss the sampling strategy shortly. We wish to construct an interpolation scheme for the elastic energy and its derivatives. Thanks to the reduced deformation model, both the energy and its derivatives are smooth, and a sufficiently dense interpolation scheme can provide a good approximation. We use BGBC as interpolation scheme, which boils down to computing the BGBC for the cubature points $\{X_i\}$ on the volumetric mesh of the soft-tissue portion of the skeletal model. Note that these BGBC are different from those of the handles introduced in Section 3.2.

Given the elastic energy density $\Psi(X)$ (and its derivatives) sampled at the cubature points, $\{\Psi(X_i)\}$, we interpolate the energy using BGBC $\{\alpha_i(X)\}$ as $\Psi(X) = \sum_i \alpha_i(X)\Psi(X_i)$. We can compute the full energy E by integrating this interpolated energy density on

Figure 9: *Our model incorporates skeletal tracking of target input animations through control forces. Note that even in the absence of external interactions, dynamic deformations appear as an effect of inertial components. The figure shows a sequence of three animation frames and a colormap with the corresponding vertex displacements in unposed space (insets).*

the whole reference shape:

$$E = \int_{\overline{T}} \sum_i \alpha_i(X)\,\Psi(X_i)\,d\overline{T} = \sum_i \left(\int_{\overline{T}} \alpha_i(X)\,d\overline{T} \right) \Psi(X_i). \quad (5)$$

Alternatively, we can define the full energy E using cubature, with cubature weights $\{w_i\}$:

$$E = \sum_i w_i\,\Psi(X_i). \quad (6)$$

Simply by equating both expressions, we see that the cubature weights can be obtained by integrating the BGBC on the reference shape.

$$w_i = \int_{\overline{T}} \alpha_i(X)\,d\overline{T}. \quad (7)$$

Our cubature method provides a good approximation of the energy and its derivatives, but it is also fast.

We have explored several strategies for sampling cubature points. One strategy was to co-locate cubature points and basis handles, and thus interpolate the internal energy and its derivatives from the same samples as the deformation field. However, internal forces are simply not uniform at the surface of rigid handles (i.e., bones); therefore, the interpolation scheme is not well defined. Another strategy was to apply importance sampling, favoring denser sampling at locations with potentially larger deformation. However, due to our approach to compute cubature weights in (7), some cubature samples with large deformation receive a large influence from regions with little deformation, leading to wrong force estimations. We concluded that uniform sampling was the safest strategy, and we found no apparent increase in quality after using 5 to 10 cubature points per basis handle.

4.3. Skeletal Constraints and Forces

Our augmented skeletal model (3) defines the skeletal DoFs θ, but we must define joint constraints and forces to correctly simulate skeletal dynamics. Furthermore, it is important that the skeletal pose remains within the observed subspace of the parametric model, otherwise the pose-dependent blend shapes will produce unnatural results. To this end, we implement the following types of skeletal forces: joint constraints to maintain the skeletal structure, joint stiffness to capture bending resistance, joint limits, and PD control forces (a.k.a. viscoelastic coupling) to enable interactive tracking and/or animation control as shown in Figure 9.

We model all skeletal forces, including joint constraints, through a combination of translation and rotational springs. These forces act only on the skeletal pose θ, with no direct effect on soft-tissue deformation ϕ.

4.4. Contact

We evaluate contact on surface points $x \in S$, which are computed according to (3) as $x = W(T(\phi,\theta),\theta)$. Recall that $W(\cdot)$ is the skinning transformation, and $T = \bar{x}(\theta) + u(\phi)$ is the unposed deformation of the reference shape. In our implementation, we define penalty contacts for colliding surface points. To transfer penalty contact forces to the DoFs of the model, we require the Jacobian of the surface position x w.r.t. the DoFs. The same Jacobian would be necessary for constraint-based contact handling.

Since surface positions depend on both the skeletal pose θ and the soft-tissue handle points ϕ, contact forces act on both the skeleton and the soft-tissue deformation. Effectively, this shared dependency plays the role of two-way coupling between skeleton and soft tissue. The Jacobians of the surface position can be computed as:

$$\frac{\partial x}{\partial \theta} = \frac{\partial W}{\partial T}\frac{\partial B_P}{\partial \theta} + \frac{\partial W}{\partial \theta}, \qquad \frac{\partial x}{\partial \phi} = \frac{\partial W}{\partial T} U_\phi. \quad (8)$$

We have observed that, in practice, the forces on the skeleton are dominated by the direct influence on the skinning transformation through $\frac{\partial W}{\partial \theta}$, with the influence through the pose blend-shapes $\frac{\partial B_P}{\partial \theta}$ negligible. To maximize performance, we have discarded the latter in our implementation. The dynamics solver also requires force Jacobians, and in particular the mixed second derivative of the skinning transformation $\frac{\partial^2 W}{\partial T \partial \theta}$. As shown in Figure 8, our contact formulation produces fast plausible simulations, allowing the use of our soft skeletal model for interactive hand tracking in contact-rich virtual environments. We refer the reader to the supplementary video for a more detailed render of these simulation scenarios.

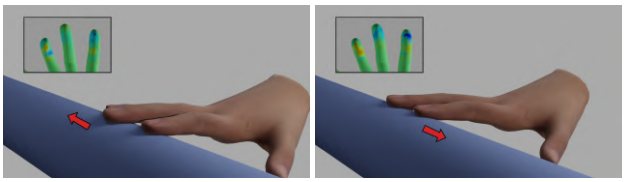

Figure 10: *Fingers sliding sideways along a cylindrical shape. The resulting deformation of the fingertips is shown in unposed reference shape. The colormap indicates the first right Cauchy-Green tensor invariant; note the difference between stretch (red) and compression (blue) at the sides of the fingertips depending on the effect of sliding direction.*

4.5. Dynamics

To simulate dynamic deformations of our augmented skeletal model, we integrate equations of motion of the form

$$M \begin{pmatrix} \ddot{\theta} \\ \ddot{\phi} \end{pmatrix} = \begin{pmatrix} f_\theta \\ f_\phi \end{pmatrix}. \tag{9}$$

We integrate the dynamic equations using backward Euler with one Newton iteration, and we achieve inertial soft-tissue deformations induced by skeletal motion, such as those in Figure 7. As discussed before, the Newton solve requires the computation of the various force Jacobians.

The bone forces f_θ include the skeletal forces described in Section 4.3. The reduced soft-tissue forces f_ϕ include the elastic forces described in Section 4.1. Contact forces affect both bone and soft-tissue forces, as described in Section 4.4. The mass matrix is derived by formulating the kinetic energy of the system. This boils down to:

$$M = \int_{\overline{T}} \frac{1}{2} \rho \begin{pmatrix} \frac{\partial x}{\partial \theta} & \frac{\partial x}{\partial \phi} \end{pmatrix}^T \begin{pmatrix} \frac{\partial x}{\partial \theta} & \frac{\partial x}{\partial \phi} \end{pmatrix} d\overline{T}, \tag{10}$$

with the Jacobians given in (8). We leverage the cubature method discussed in Section 4.2 to approximate the mass matrix, with one modification: we must add the inertia terms of the bones to the mass matrix computed on the volumetric mesh.

5. Results

The soft skeleton model presented above provides a general scheme to augment any arbitrary PSD with soft-tissue deformations. The resulting method features realistic dynamics, highly non-linear materials, and two-way coupling between flesh and bones through frictional contact and inertia. While any other PSD could be potentially used, our method gets the most from parametric models. As global static deformations are handled by the data-driven pose blend shapes, the subspace basis is completely devoted to representing local deformations. In this section, we describe in more detail the SMPL and MANO models and present some results.

5.1. Augmented MANO

The MANO model represents the hand as a template triangle mesh of $n = 3106$ vertices and 6208 faces. Static skin deformations are parameterized through $s = 10$ shape parameters and $p = 96$ pose parameters. Shape parameters are kept constant during simulation and allow to personalize the hand model for different users. We optimized shape parameters to fit a real hand model of an adult male of 50th percentile height and weight obtained using CT and MRI data. Pose parameters determine the configuration of the 16 bones and 15 joints of the skeletal model and produce the corresponding pose-space deformations through pose blend shapes.

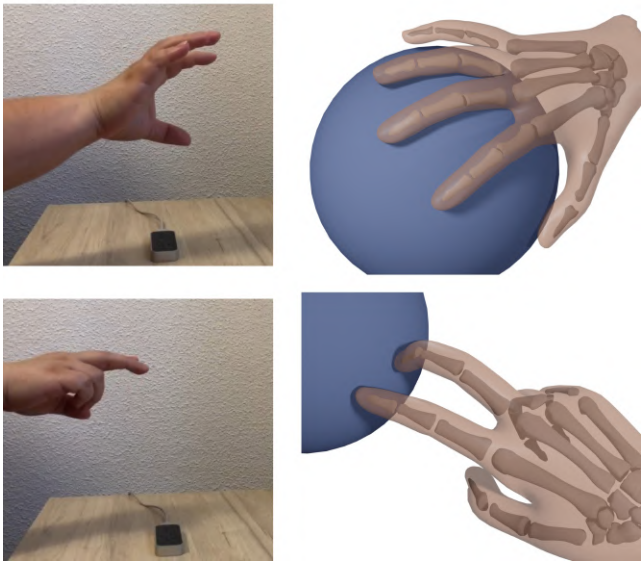

Figure 11: *Interactive hand tracking demo using the Leap Motion. The user is capable of touching and grasping environment objects, producing significant soft-tissue deformations as an effect of frictional contact.*

To augment MANO we first define the volumetric mesh of the soft-tissue layer. We represent the surface of each bone with a triangle mesh comprising a total of 10000 nodes and 19898 faces. Then, we use TetGen to generate a tetrahedral mesh conformal to both skin and bone meshes, which leads to a total of 20214 nodes and 88716 elements. Simulating the full space of 60642 DoFs would be infeasible for interactive applications. Thus, we build our subspace basis by manually distributing $h = 87$ handle points throughout the palm of the hand, where the main contact interaction is expected to happen. Together with the skeleton root and joint angles, this leads to a total of 357 simulated DoFs. In order to approximate soft-tissue forces and Jacobians with our BGBC cubature scheme, we found 700 integration points to be sufficient.

As shown in Figure 8 and Figure 10, the resulting skeletal model produces realistic soft-tissue deformations due to frictional contact with environment objects. The whole simulation runs in real-time which allows us to integrate interactive hand tracking using the Leap Motion (Figure 11).

5.2. Augmented SMPL

The SMPL model is defined analogously to the MANO model. The template mesh is composed of $n = 6890$ vertices and 13776 faces,

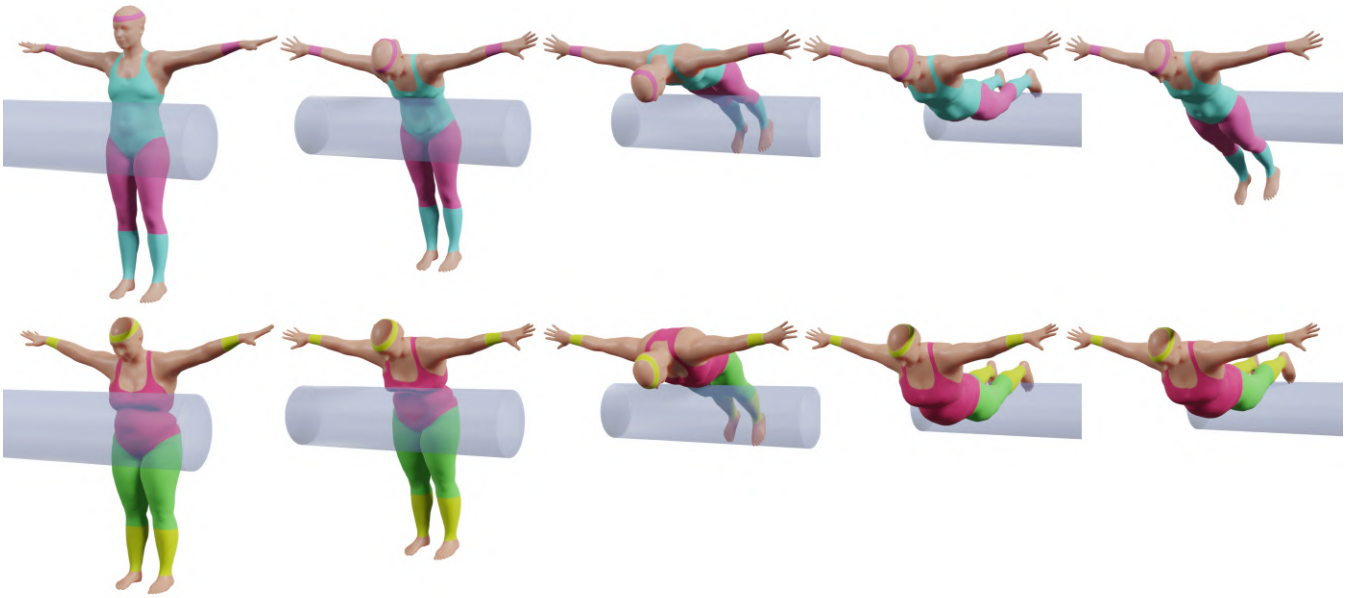

Figure 12: *Each row presents a sequence of pictures showing two rag-doll characters with different shape parameters undergo the same simulation scenario. The bodies are slowly pushed by a cylinder while hanging from the wrists, resulting in different deformation behaviors.*

whose deformation is controlled by $s = 10$ shape parameters and $p = 144$ pose parameters. To define the soft-tissue layer, we follow the approach described in [ROCP20]; here, the inner surface is defined by displacing the vertices of the template mesh a distance given by a layer thickness value that varies throughout the body. The resulting tetrahedral mesh conformal to such boundary surfaces comprises a total of 10111 nodes and 41585 elements, 500 of which are selected as cubature integration points. Finally, we manually sample $h = 82$ handle points uniformly distributed throughout the surface of the body which leads to a total of 672 simulated DoFs.

Figure 13: *We compare the behavior of our method (top) against the ground-truth full-space problem (bottom). While the full-space solution is slightly smoother, our approximation produces a plausible behavior at a computational cost orders of magnitude lower.*

As shown in Figure 6, the resulting skeletal model accurately matches data-driven static deformations while at the same time realistically responding to external interactions. The deformation of the skeleton can be driven by an input animation through tracking forces (Figure 9), and the soft-tissue dynamically deforms accordingly due to the effect of inertial forces (Figure 7). Interestingly, as shown in Figure 12, the parametric model allows us to reproduce

		force	Hessian	solve	step
MANO	full space	1119	2928	6883	10932
	subspace 700	1.01	10.24	0.51	11.78
	subspace 2000	1.87	16.4	0.53	18.82
SMPL	full space	882	2401	3947	7233
	subspace 500	1.51	7.16	0.49	9.17
	subspace 1400	1.99	11.63	0.47	14.1

Table 1: *Performance comparison of a full-space simulation vs. our method, with different numbers of cubature points (denotes as "subspace X"). The table shows average timings per time step, as well as broken down into the evaluation of forces, the evaluation of the energy Hessian, and the linear system solve (all in ms).*

Figure 14: *We compare our handle basis (center) and a modal basis (right) on the augmented MANO model. As reference, we also show the same scene without soft-tissue deformation (left). The modal basis has difficulty producing the correct bulging on the side of the hand, and it suffers artifacts on the finger tips, far from the contact area, due to the global support of the basis.*

the same simulation scenarios for different body shapes resulting in different deformation behaviors.

5.3. Performance

All our experiments have been performed on a laptop machine Intel Core i7-9750H @ 2.6GHz, with 32GB RAM. On average, simulations run at close to 100 FPS allowing us to interactively manipulate the simulated objects. Figure 13 shows a comparison of the deformation behavior obtained by solving the same simulation scenario considering the full-space problem and our subspace approximation. While differences are noticeable, our soft skeleton model produces plausible behaviors while running in real-time. In comparison, solving the full space problem takes around 7 seconds per frame on the augmented SMPL model, and over 10 seconds per frame on the augmented MANO model. We refer the reader to the supplementary video for additional simulation results.

Table 5.2 shows a breakdown of timings, comparing a full-space simulation, our subspace method with the number of cubature points used in the examples, and our method with more cubature points. The subspace formulation provides a speed-up of over 1000× on the linear system solve of each time step. On the other hand, cubature integration provides a speed-up of almost 400× on the evaluation of forces and the energy Hessian. We confirm that the force and Hessian evaluations scale sublinearly with the number of cubature points.

5.4. Comparison to Modal Basis

One of the major features of our model is the choice of a handle basis for the subspace representation, which ensures a good balance between local support and the size of the basis. As a representative global basis that requires no training data, we have tested our method with modal analysis. For the augmented MANO model shown in Figure 14 we used 261 modes, and for the augmented SMPL model shown in Figure 15 we used 246 modes. In both cases, the number of modes is three times the number of handles, to retain the same number of DoFs.

We draw two major conclusions from these comparisons. First, the handle basis represents deformations induced by contact much more accurately, as it avoids the issues induced by the global support of the modal basis (see artifacts at finger tips in Figure 14 and at the elbow in Figure 15). Second, the modal basis needs many more cubature points to avoid artifacts. Modes of moderate

Figure 15: *We compare our handle basis (right) and a modal basis (left) on the augmented SMPL model, as a sphere presses the chest of the avatar. Our model resolves the contact smoothly, while the modal basis suffers artifacts both close to the contact and far, in the arm and the elbow.*

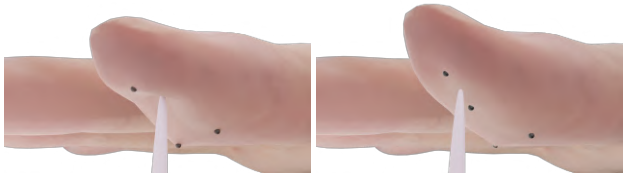

Figure 16: *The density of handles determines the ability to resolve contacts with high spatial frequency. In the images, we press a finger pad of the augmented MANO model with a pin, and we show the handles in black. The contact is resolved more accurately as the pin approaches a handle (left), and smoothly degrades as the pin moves away from the handles (right).*

frequency, which are needed for a good representation of contact deformations, may produce deformation spikes that go unnoticed by cubature integration. In the augmented MANO model, we increased the number of cubature points from 700 (with the handle basis) to 2000 (with the modal basis), otherwise the artifacts at finger tips were ridiculous. With 261 modes and 700 cubature points, performance dropped to 1.2 FPS (compared to 85 FPS with our handle basis), due to the global support. With 2000 cubature points, performance was as low as 0.9 FPS, although our implementation may not be as efficient for a global basis.

6. Conclusions and Future Work

We have presented a method to augment skeletal animation models with subspace soft-tissue deformations. Our method enjoys important practical benefits, as it allows easy design of a subspace basis and a subspace integration method without the need for deformation examples. We have integrated it with two popular data-driven animation models for bodies and hands, effectively augmenting these models with interactive soft-tissue deformations. However, our method is not free of limitations. Most of these limitations stem from two choices of the method: the unposed deformation space and the subspace representation.

By measuring deformations in the unposed reference space, we suffer errors in the estimation of the deformation gradient. Some of these errors are actually intended, and they help the model reach the data-driven pose without causing internal stress. But other errors may alter the expected behavior of the material model. This occurs particularly near joints, where the skinning transformation from unposed to posed space deviates most from a rigid transformation. With our nonlinear material, this deviation may induce overestimation or underestimation of the saturation term. We believe, however, that the benefits of the unposed deformation metric surpass its limitations. One additional benefit is the robustness under large joint rotations. The unposed formulation avoids mesh degeneracies that are otherwise commonplace near joints. As shown in Figure 4, we can mesh a soft-tissue layer that conforms accurately to the geometry of skeletal bones.

The use of a subspace deformation evidently limits the range of possible deformations, of course with the benefit of computational efficiency. Figure 16 highlights the limitation to accurately resolve contacts with high spatial frequency. One way to alleviate this limitation is to enrich the subspace basis at runtime. It is worth exploring the application of existing enrichment methods [HZ13,TMDK15] to our skinning-based reduced model. In our particular choice of subspace basis, we have focused the placement of handle points on the surface of the model. However, one could consider adding handle points within the volume to capture internal heterogeneity. In the construction of our subspace cubature integration, we have used uniform sampling, but a better cost-to-accuracy trade-off might be possible with the addition of importance sampling. Last, although not explored in our work, the subspace model can be further improved by adapting it in pose space [XB16].

Beyond limitations of the method, our work could also be further extended to address limitations of the demonstration examples. Our simulation engine does not support two-way coupling with other simulated objects, collisions with deformable objects, or self-collisions. Nothing prevents incorporating these features; however, self-collision handling might become the bottleneck of the simulation. To retain the efficiency of the method, it might be necessary to include subspace handling of self-collisions [TOK14].

Acknowledgements

The authors would like to thank the reviewers for their time and helpful feedback; Suzanne Sorli, for her help with Leap Motion setup; Rosa Sánchez and Igor Santesteban, for help with the preparation of results and also other members of the MSLab at URJC for their support. This work was funded in part by the European Research Council (ERC Consolidator Grant no.772738 TouchDesign) and the Spanish Ministry of Science (RTI2018-098694-B-I00 VizLearning)

References

[AKJ08] AN S. S., KIM T., JAMES D. L.: Optimizing cubature for efficient integration of subspace deformations. *ACM Trans. Graph. 27*, 5 (2008). 2, 3, 6

[BEH18] BRANDT C., EISEMANN E., HILDEBRANDT K.: Hyper-reduced projective dynamics. *ACM Trans. Graph. 37*, 4 (2018). 3, 4

[BJ05] BARBIČ J., JAMES D. L.: Real-time subspace integration for st. venant-kirchhoff deformable models. *ACM Trans. Graph. 24*, 3 (July 2005), 982–990. 2

[BS19] BARGTEIL A. W., SHINAR T.: An introduction to physics-based animation. In *ACM SIGGRAPH 2019 Courses* (New York, NY, USA, 2019), SIGGRAPH '19, Association for Computing Machinery. 2

[BZ11] BARBIČ J., ZHAO Y.: Real-time large-deformation substructuring. In *ACM SIGGRAPH 2011 Papers* (New York, NY, USA, 2011), SIGGRAPH '11, Association for Computing Machinery. 3

[CBC*05] CAPELL S., BURKHART M., CURLESS B., DUCHAMP T., POPOVIĆ Z.: Physically based rigging for deformable characters. In *Proceedings of the 2005 ACM SIGGRAPH/Eurographics Symposium on Computer Animation* (New York, NY, USA, 2005), SCA '05, Association for Computing Machinery, p. 301–310. 2

[CGC*02] CAPELL S., GREEN S., CURLESS B., DUCHAMP T., POPOVIĆ Z.: Interactive skeleton-driven dynamic deformations. *ACM Trans. Graph. 21*, 3 (July 2002), 586–593. 2

[FGBP11] FAURE F., GILLES B., BOUSQUET G., PAI D. K.: Sparse meshless models of complex deformable solids. *ACM Trans. Graph. 30*, 4 (July 2011). 3

[FMD*19] FULTON L., MODI V., DUVENAUD D., LEVIN D., JACOBSON A.: Latent-space dynamics for reduced deformable simulation. 2

[GBFP11] GILLES B., BOUSQUET G., FAURE F., PAI D. K.: Frame-based elastic models. *ACM Trans. Graph. 30*, 2 (Apr. 2011). 3, 4

[GOM*09] GALOPPO N., OTADUY M. A., MOSS W., SEWALL J., CURTIS S., LIN M. C.: Controlling deformable material with dynamic morph targets. In *Proceedings of the 2009 Symposium on Interactive 3D Graphics and Games* (New York, NY, USA, 2009), I3D '09, Association for Computing Machinery, p. 39–47. 2, 3

[GOT*07] GALOPPO N., OTADUY M. A., TEKIN S., GROSS M., LIN M. C.: Soft articulated characters with fast contact handling. *Computer Graphics Forum 26*, 3 (2007), 243–253. 2

[HMT*12] HAHN F., MARTIN S., THOMASZEWSKI B., SUMNER R., COROS S., GROSS M.: Rig-space physics. *ACM Trans. Graph. 31*, 4 (July 2012). 2

[HTC*13] HAHN F., THOMASZEWSKI B., COROS S., SUMNER R. W., GROSS M.: Efficient simulation of secondary motion in rig-space. In *Proceedings of the 12th ACM SIGGRAPH/Eurographics Symposium on Computer Animation* (New York, NY, USA, 2013), SCA '13, Association for Computing Machinery, p. 165–171. 2

[HTC*14] HAHN F., THOMASZEWSKI B., COROS S., SUMNER R. W., COLE F., MEYER M., DEROSE T., GROSS M.: Subspace clothing simulation using adaptive bases. *ACM Trans. Graph. 33*, 4 (July 2014). 3

[HZ13] HARMON D., ZORIN D.: Subspace integration with local deformations. *ACM Trans. Graph. 32*, 4 (July 2013). 3, 11

[KJ11] KIM T., JAMES D. L.: Physics-based character skinning using multi-domain subspace deformations. In *Proceedings of the 2011 ACM SIGGRAPH/Eurographics Symposium on Computer Animation* (New York, NY, USA, 2011), SCA '11, Association for Computing Machinery, p. 63–72. 3

[KJP02] KRY P. G., JAMES D. L., PAI D. K.: Eigenskin: Real time large deformation character skinning in hardware. In *Proceedings of the 2002 ACM SIGGRAPH/Eurographics Symposium on Computer Animation* (New York, NY, USA, 2002), SCA '02, Association for Computing Machinery, p. 153–159. 3

[KLM01] KRYSL P., LALL S., MARSDEN J. E.: Dimensional model reduction in non-linear finite element dynamics of solids and structures. *International Journal for Numerical Methods in Engineering 51*, 4 (2001), 479–504. 2

[KPMP*17] KIM M., PONS-MOLL G., PUJADES S., BANG S., KIM J., BLACK M. J., LEE S.-H.: Data-driven physics for human soft tissue animation. *ACM Transactions on Graphics (TOG) 36*, 4 (2017), 54. 2, 4

[LCF00] LEWIS J. P., CORDNER M., FONG N.: Pose space deformation: A unified approach to shape interpolation and skeleton-driven deformation. In *Proceedings of the 27th Annual Conference on Computer Graphics and Interactive Techniques* (USA, 2000), SIGGRAPH '00, ACM Press/Addison-Wesley Publishing Co., p. 165–172. 2, 3

[LLK19] LI J., LIU T., KAVAN L.: Fast simulation of deformable characters with articulated skeletons in projective dynamics. In *Proceedings of the 18th Annual ACM SIGGRAPH/Eurographics Symposium on Computer Animation* (New York, NY, USA, 2019), SCA '19, Association for Computing Machinery. 2

[LMR*15] LOPER M., MAHMOOD N., ROMERO J., PONS-MOLL G., BLACK M. J.: Smpl: A skinned multi-person linear model. *ACM Trans. Graph. 34*, 6 (Oct. 2015), 248:1–248:16. 2, 3

[LYWG13] LIU L., YIN K., WANG B., GUO B.: Simulation and control of skeleton-driven soft body characters. *ACM Trans. Graph. 32*, 6 (Nov. 2013). 2

[MTLT89] MAGNENAT-THALMANN N., LAPERRIÈRE R., THALMANN D.: Joint-dependent local deformations for hand animation and object grasping. In *Proceedings on Graphics Interface '88* (CAN, 1989), Canadian Information Processing Society, p. 26–33. 2, 3

[MZS*11] MCADAMS A., ZHU Y., SELLE A., EMPEY M., TAMSTORF R., TERAN J., SIFAKIS E.: Efficient elasticity for character skinning with contact and collisions. *ACM Trans. Graph. 30*, 4 (July 2011). 2

[NMK*06] NEALEN A., MÜLLER M., KEISER R., BOXERMAN E., CARLSON M.: Physically based deformable models in computer graphics. *Computer Graphics Forum 25*, 4 (2006), 809–836. 2

[NVW*13] NEUMANN T., VARANASI K., WENGER S., WACKER M., MAGNOR M., THEOBALT C.: Sparse localized deformation components. *ACM Trans. Graph. 32*, 6 (Nov. 2013). 3

[OHS03] O'BRIEN J., HAUSER K., SHEN C.: Interactive deformation using modal analysis with constraints. *Graphics Interface 3* (05 2003). 2

[PCH*13] PEREZ A. G., CIRIO G., HERNANDEZ F., GARRE C., OTADUY M. A.: Strain limiting for soft finger contact simulation. In *2013 World Haptics Conference (WHC)* (2013), pp. 79–84. 6

[ROCP20] ROMERO C., OTADUY M. A., CASAS D., PEREZ J.: Modeling and estimation of nonlinear skin mechanics for animated avatars. *Computer Graphics Forum (Proc. Eurographics) 39*, 2 (2020). 2, 4, 6, 9

[RTB17] ROMERO J., TZIONAS D., BLACK M. J.: Embodied hands: Modeling and capturing hands and bodies together. *ACM Trans. Graph. 36*, 6 (2017). 2, 3

[SB12] SIFAKIS E., BARBIC J.: Fem simulation of 3d deformable solids: A practitioner's guide to theory, discretization and model reduction. In *ACM SIGGRAPH 2012 Courses* (2012), pp. 20:1–20:50. 2, 6

[Si15] SI H.: Tetgen, a delaunay-based quality tetrahedral mesh generator. *ACM Trans. Math. Softw. 41*, 2 (Feb. 2015), 11:1–11:36. 4

[TMDK15] TENG Y., MEYER M., DEROSE T., KIM T.: Subspace condensation: Full space adaptivity for subspace deformations. *ACM Trans. Graph. 34*, 4 (July 2015). 2, 3, 11

[TOK14] TENG Y., OTADUY M. A., KIM T.: Simulating articulated subspace self-contact. *ACM Trans. Graph. 33*, 4 (July 2014). 11

[TW88] TERZOPOULOS D., WITKIN A.: Physically based models with rigid and deformable components. *IEEE Computer Graphics and Applications 8*, 6 (1988), 41–51. 2

[vTSSH13] VON TYCOWICZ C., SCHULZ C., SEIDEL H.-P., HILDEBRANDT K.: An efficient construction of reduced deformable objects. *ACM Trans. Graph. 32*, 6 (2013). 3, 6

[WJBK15] WANG Y., JACOBSON A., BARBIČ J., KAVAN L.: Linear subspace design for real-time shape deformation. *ACM Trans. Graph. 34*, 4 (2015). 2, 3, 4

[XB16] XU H., BARBIČ J.: Pose-space subspace dynamics. *ACM Trans. Graph. 35*, 4 (July 2016). 2, 3, 11